Arabian Journal for Science and Engineering (2021) 46:12613–12623
https://doi.org/10.1007/s13369-021-06000-z

RESEARCH ARTICLE-MECHANICAL ENGINEERING

# The Effect of TIG Welding Parameters and Automatization for Non-Heat Treated Inconel 718 Sheets

**Akay Nevcanoğlu**[1] · **Yahya Bozkurt**[1] · **Serdar Salman**[2]

Received: 22 February 2021 / Accepted: 8 July 2021 / Published online: 11 August 2021


## Abstract

Inconel 718 alloy is widely used in applications that require advanced strength properties especially at high temperature conditions. Combust room walls, exhaust parts, jet tribune blades and gas tribune equipment are the most known using areas. This alloy can be welded with various fusion welding methods, but TIG (Tungsten Inert Gas) welding is preferred since, it provides simply application, mobility and low cost. This study was aimed to clarify that how adjusting the welding parameters and welding automatically can help to achieve promising mechanical properties before heat treatments. The welding experiments were conducted on three different welding current values and attention was paid to provide full penetration for each condition. The results showed that the highest welding current value which did not cause welding defects lead to decrease heat input due to the high transverse speed usage. Moreover, by automatically welding, the heat input was decreased to a minimum level that provided excellent tensile strength and elongation properties. Dendrites turned to cellular from colon. Hazardous zones, such as HAZ and PMZ, narrowed down. The Laves phase ratio and grain size also decreased. Microhardness results confirmed these microstructure observations. The crack observations after tensile tests showed that failures were near HAZ in high-heat input conditions. However, failures were observed in FZ for low-heat input conditions. Additionally, ductile fracture and fracture similar to cleavage mechanisms were observed together due to adjusting the parameters and automatization.

**Keywords** Inconel 718 · TIG welding · Automatic welding · Welding microstructure · Mechanical properties · Fracture mechanism

## 1 Introduction

Inconel 718 is a nickel-based austenitic super alloy, which is used in airplanes, rockets, ships, locomotives, power plants in gas turbines and in various places of petroleum. Inconel 718 suits in applications where high strength is required between 760 and 982 °C. Jet tribune knife discs which are called "blisk" (bladed disk) can be also produced from this material (Fig. 1). Blisks are stretched 200 MPa longitudinally at temperatures up to 1100 °C. The turbine blade foot reaches 700 °C and the tensile stress can reach to 500 MPa. Inconel 718 can be welded by various fusion welding methods [1].

Many researches were made about the effect of welding parameters and automatization on last decades. Q. Wang et al. showed that weld pool width and root depth change by increasing welding current while working with another nickel-based super alloy that is GH99 [3]. They determined the welding current and transverse speed as very crucial by observing defects after welding. Several studies and industrial applications [3–6] show that the mechanical properties are linked with directly the welding parameters. Schirra et al. found that grain size affects the Laves phase fraction on non-welded Inconel 718. The specimens were on cast, wrought or HIP (Heat Isotactic Press) form. They indicated that the Laves phase arises over 982 °C and the Laves phase fraction can be controlled by heating time and temperature.

✉ Akay Nevcanoğlu
akay.nevcanoglu@marmara.edu.tr

Yahya Bozkurt
ybozkurt@marmara.edu.tr

Serdar Salman
ssalman@marmara.edu.tr

[1] Faculty of Technology, Marmara University, Istanbul, Turkey

[2] National Defence University, Istanbul, Turkey

**Fig. 1** Blisks, made of Inconel 718 with Additive Manufacturing [2]

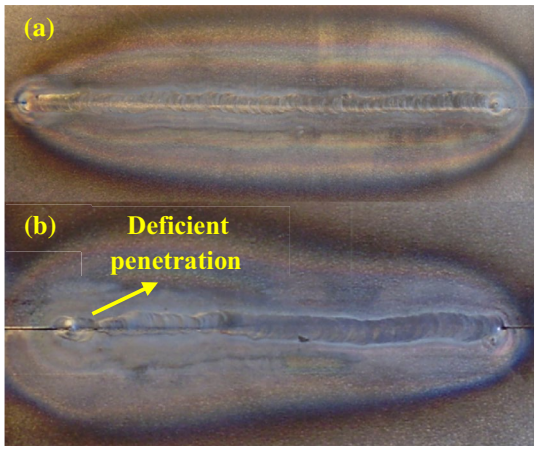


**Fig. 2** **a** Welded with robot assistance **b** Manual welded [11]

Fusion welding methods cause extreme temperatures, so the Laves phase occurring and grain size cannot be controlled while welding. The Laves phase ratio can be decreased with Post Welding Heat Treatment (PWHT) but it is preferred to never occur [7]. The well-adjusted welding parameters and suitable automatization was not considered before PWHT on their work. It was ignored that could be decreased the Laves phase ratio, if they adjusted accurately the welding parameters. Many researchers [5–9] prefer welding methods which are worked higher current density such as Electron Beam Welding (EBW) and Laser Welding (LW) due to the lower heat input and narrower heat affected zone (HAZ) owing to higher transverse speed. Nevertheless, TIG welding is preferred over other welding methods because of its low cost and simple application. It is clear that the repairing or restoring the machine parts require mobile and simple welding equipment. TIG welding maintains being first choice especially welding of damaged Inconel 718 parts. T. S. Hong et al. have studied automatic welding systems in detail [10]. They showed that narrower weld seam and homogenous welding are possible. Welding parameters could be adjusted automatically but mechanical properties that the parameters caused were not investigated. It was investigated by Erden and Maric that two pieces of 4 mm thick blank steel St-37 were welded as manual by novices and with robot assistance [11]. Weld seam was more homogeneous and stable when welding was conducted with robotic systems that can be observed in Fig. 2a. Full penetration was not provided on the manually welded specimen as seen in Fig. 2b. Kumar et al. mixed $Cr_2O_3$, FeO, and $MoO_3$ oxide fluxes to increase penetration on Inconel 718 parts. The powders were added to the mix equally. It was noticed that using fluxes can quintuplicate the penetration depth. Additionally, it was seen minimum distortion because arc stability and width were better. Therefore, the mechanical properties and hardness were increased. Hardness in the weld centre increased from 236 to 265 HV. Stress elongation has decreased %7, while tensile strength increased %35 [12]. Although these improvements on mechanical properties are found effective, flux usage increases costs, and weld seam corrosion should be controlled. Flux usage is not effective for some welding positions, such as overhead, edges and corners. Ram et al. have investigated the effect of current pulsing on TIG welding of Inconel 718. Current pulsing resulted in refined grains and basically decreased Laves phase ratio. They have described the FZ, partially melted zone (PMZ), and HAZ transformed to visible state on microstructure observations [13]. The effect of current pulsing is not understood deeply and it is needed widely researches due to fusion welding of Inconel 718.

The mechanical properties of TIG welding products are affected by heat input dramatically. High heat input leads to low strength and hardness due to more cooling time. Welding voltage (V), current (I), and transverse speed (S) are determining parameters of heat input. The energy that is provided by the welding machine is not wasted just by welding. An important amount of energy is wasted on radiation and heating workpiece due to method losses. The amount of energy that is used while welding is determined by energy efficiency (η). Energy efficiency is variable for every welding method and it is %70 for TIG welding. The heat input formula is shown as in Eq. 1. Heat input affects cooling time and cooling ratio, so it has an important role for mechanical properties [14, 15].

$$H = \frac{V \times I \times \eta \times 60}{S}$$

The purpose of this article is to present optimum welding parameters before PWHT to reveal the real effect of welding parameters especially to be a guide for welding operators to prepare providing the best properties on their works. Although TIG welding of Inconel 718 was widely researched by previous researchers, there is not enough information about how the mechanical properties and microstructure

**Table 1** Chemical composition of Inconel 718 sheet (mass fraction: %) [20]

| | C | Mn | P | S | Si | Cr | Ni | Mo | Nb | Ti | Al | Fe | Co |
|---|---|---|---|---|---|---|---|---|---|---|---|---|---|
| Min | – | – | – | – | – | 17 | 50 | 2.8 | 4.75 | 0.65 | 0.2 | Balance | – |
| Max | 0.08 | 0.35 | 0.015 | 0.015 | 0.35 | 21 | 55 | 3.3 | 5.5 | 1.15 | 0.8 | Balance | 1 |

**Table 2** Mechanical properties of Inconel 718 sheet [20]

| Yield strength (MPa) | Tensile strength (MPa) | Microhardness (HV) |
|---|---|---|
| 725 | 1035 | 214.75 |

can be advanced due to adjusting welding parameters and automatization. In addition, this article presents an approach about the interrelation between heat input and work piece thickness, which is generally determined due to experience of welding operator. HAZ, PMZ and FZ microstructures of specimens were examined and they were associated with microhardness and tensile properties. The Laves phase ratio and grain size changes were observed on microstructure and associated with welding parameters. Additionally, fractured surfaces were analysed and related with tensile test results.

## 2 Experimental studies

The dimensions of 30 × 60 mm and 1 mm thick Inconel 718 sheets were welded manually and automatically by TIG adopted milling machine according to TS EN ISO 5817:2014 standards to provide the same welding distances [16]. A special fixture made of copper material was designed to eliminate distortions while welding. According to TS EN ISO 6848 standards, WC20, 2.4 × 175 mm, tungsten electrodes were used [17]. Tensile test specimens were prepared according to ASTM E8/E8M-09 standards [18]. The specimens have been extracted by a software-controlled laser cutting machine to minimalize the heat effect. Additionally, rectangular parts were extracted from the sheets to use on microhardness tests. They were polished using conventional polishing methods and chemically etched with Glyceregia 87 according to ASTM E-407-07(2015)e1 standards [19]. This solution includes 15 ml HCl, 10 ml glycerine and 5 ml $HNO_3$ approximately. Tensile test specimens and rectangular parts for microstructure observations were extracted from welded sheets by laser cutting machine. The chemical composition and mechanical properties of the Inconel 718 sheet are given in Tables 1 and 2, respectively.

Welding parameters were mainly determined based on our previous study [21] and Anuradha et al. [22]. In present work, the current usage under 30 A and upper 80 A caused undesired results for 1 mm thick Inconel 718 sheets as shown in Fig. 3a and b. The transverse speed was adjusted

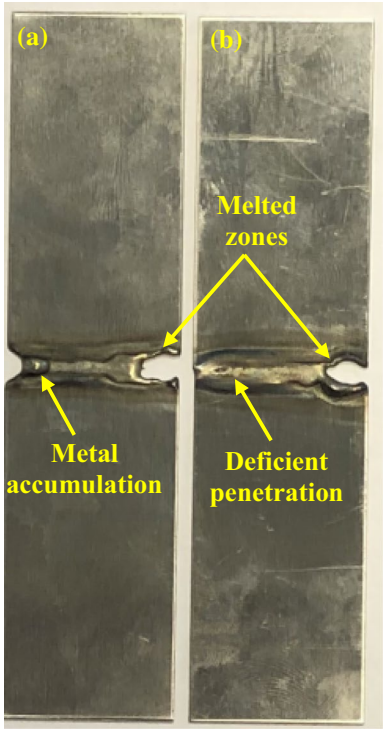


**Fig. 3** **a** 20 A and **b** 100 A manually welded specimens

due to the full penetration throughout the weld seam for each work piece. It was used direct current electrode negative (DCEN) and 220 Volt energy. Alternative current (AC) and direct current electrode positive (DCEP) are rarely preferred for Inconel 718 welding on the literature [22–24]. DCEN provided better weldability compared with AC and DCEP. It was selected 12 l/min argon as shielding gas for all conditions to provide same welding atmosphere. The parameters were selected randomly, but in the appropriate range for 1 mm thickness [21]. All sheets were welded at one pass without filler metal. The welding parameters used in this study are listed in Table 3. The parameters are adjusted to minimize the conventional defects such as microfissuring, the Laves phase occurring, distortions, and melted areas in weld seam.

Manual welding required extra attention to adjust parameters, such as arc distance, transverse speed, and torch angle. All the manual weldments were completed by the same welding operator. The continuous current was preferred and no fluxes were used to understand the real effect of current properties. In automatic welding, torch angle was selected

**Table 3** The welding parameters

| Specimen | Welding current (I-A) | Transverse speed (mm/min) | Gas flow (l/min) | Arc distance (mm) | Torch angle (°) |
|---|---|---|---|---|---|
| 1 | 30 | 126 | 12 | Manual | Manual |
| 2 | 50 | 245 | 12 | Manual | Manual |
| 3 | 80 | 453 | 12 | Manual | Manual |
| 4 | 80 Auto | 548 | 12 | 2.40 | 70 |

70° as observed on manual welding torch angle. Microstructural examinations were conducted with an optical microscope (OM) and scanning electron microscope (SEM). OM was Olympus BX51M model and SEM was FEI XL-30 model. Vickers microhardness tests were performed with a Future-Tech, FM-310e machine using 200 gf load for 10 s. Tensile strength tests were conducted with the Devotrans D.V.T. model machine. It can apply 50 kN force maximum capacity. Tensile strength tests were conducted at 0.5 mm/min speed.

OM and SEM were used to show general view of weld seam, different weld zones, and changes on grain shapes and sizes. Additionally, their software enabled to measure the width of zones. SEM was also used to analyse fractography properties. Microhardness tests were conducted with least five measures in every welding zone. It was paid attention to let required distances between measuring points by OM of microhardness machine. Tensile tests completed in same day to intercept atmosphere differences such as; temperature and humidity. Three tensile specimens were tested for each condition and their average test results were noted.

## 3 Results and discussions

### 3.1 Macro observation

Most of the studies on TIG welding of Inconel 718 are mainly about joining sheets thicker than 1 mm. It is observed that current values have been generally preferred up to 150 A and DCEN was decided as the current type [3, 12, 25, 26]. In our study, current values lower than 30 A resulted in metal accumulation on weld seam and distortion existed on sheets due to excess heat. Current values higher than 80 A resulted in deficient penetration, because of extreme transverse speed. When the transverse speed was decreased on 100 A welded sheets, same defects were observed that were detected on 20 A welded sheets [13, 15]. This evidence could be seen as macroscopic on 20 A and 100 A manually welded specimens as shown in Fig. 3a and b. Additionally, it was difficult to adjust the first spark for all specimens.

A special fixture was designed to minimize the distortions; even so, these two specimens were exposed to distortions which could not be defeated anyway. The first spark in 100 A specimens led to big holes at every try, in fact, sometimes they existed in the middle of weld seam. This fact made welding impossible on 100 A, because it could not be obeyed by standards of TS EN ISO 5817:2014 [16]. Melted zones on 20 A specimens were generally at the starting of the weld seam because this current value required more time to combining two sheets at the starting than the whole work. This evidence also showed that these current values could not able to automatization, for 1 mm thick Inconel 718 sheet.

### 3.2 Heat input

Low welding current usage led to deficient penetration if transverse speed was not decreased as shown in Table 3. Heat input increased %35 when transverse speed was adjusted due to provide full penetration. Heat input was decreased by elevating current that can be observed in Table 4. Agilan et al. focussed on effect of heat input for welding of Inconel 718 sheets with EBW. They affirmed that the weld metal cooling rate dramatically changed with heat input. They also detected microfissuring on the specimen even with lowest heat input [6]. These results can be amendable by adjusting transverse speed. Transverse speed was adjusted depending on welding current in order to provide best mechanical properties for each specimen in present work. Excess heat leads to several problems on Inconel 718, which is reason of low transverse speed or high current usage, such as niobium segregation, related to the hazardous Laves phase and microfissuring in HAZ. Additionally, because of grain growth, excess heat is not desired. Coarse grains lead to unfavourable mechanical properties except creeping strength. Heat input could be minimized due to automatic welding [4, 5, 27].

Heat input data pointed out that, it was better to work higher current which did not let to distortions or melted

**Table 4** Heat input data

| Specimen | Current (A) | Heat input (j/mm) |
|---|---|---|
| 1 | 30 | 2200.00 |
| 2 | 50 | 1885.71 |
| 3 | 80 | 1631.79 |
| 4 | 80 Auto | 1348.91 |

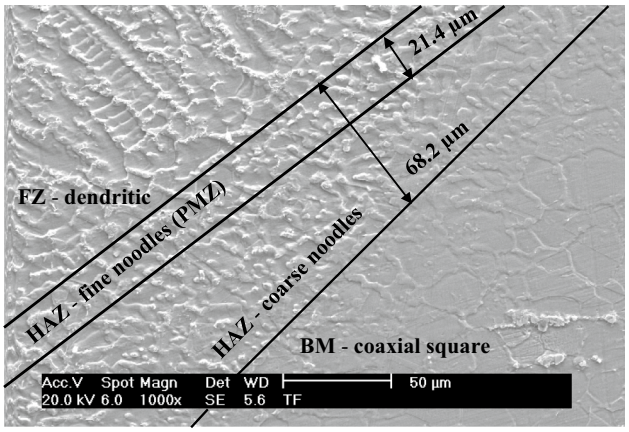


**Fig. 4** Microstructure from BM to FZ on 80 A manually welded specimen

zones on the weld seam owing to lower heat input. Actually, these heat input data (Table 4) can be taken as a reference for all Inconel 718 sheet welding works because of its 1 mm thickness. With elevating thickness on manual welding, current values can be adjusted owing to Table 4 by future researchers.

### 3.3 Microstructure

Different zones were detected from FZ to base metal (BM) on all specimens. HAZ is generally described as two sections including fine and coarse noodles by several researchers that is shown in Fig. 4 [5, 6, 15, 25]. BM had coaxial squares and FZ had dendritic shape as expected.

FZ—BM crossing microstructure of 80 A manually welded specimen, which has captured with a high-resolution SEM, pointed out that HAZ narrowed as compared with 30 and 50 A specimens. This fact resulted in a microstructure as shown in Fig. 4. HAZ width was measured as 68.2 µm. A narrow fine noodle—HAZ (PMZ) was observed. PMZ is known as the most rigid part of the weld seam that occurs due to extreme heat input. PMZ width was measured as 21.4 µm on 80 A welded specimen. The 30 A welded specimen had a wide section of PMZ and irregular grains on weld seam. PMZ on 30 A welded specimen is shown in Fig. 7 [13, 25, 28]. The microstructure of FZ had a dendritic shape on all specimens. It is shown in Fig. 5. It was observed that FZ dendrite size was reduced with heat input. Dendrite type was changing to cellular from colon. There were bright zones between the dendrites. These zones were observed easier on colon dendrites than cellular. The brighter zones are characterised as the Laves phases [6, 7, 24, 25].

Decreasing of the grain size is an expected phenomenon with decreasing heat input. Growing of the dendrites gets difficult due to rapid cooling [14, 29, 30]. It is observed that the Laves phase ratio and grain size reduced. Dendrite size increased as it was gone from FZ to HAZ. There were colon dendrites that turned into cellular dendrites. This fact was seen on 80 A manually welded specimen clearly as shown in Fig. 6.

Dendrite shape and size affect the mechanical properties of the material. Cellular dendrites serve more strength

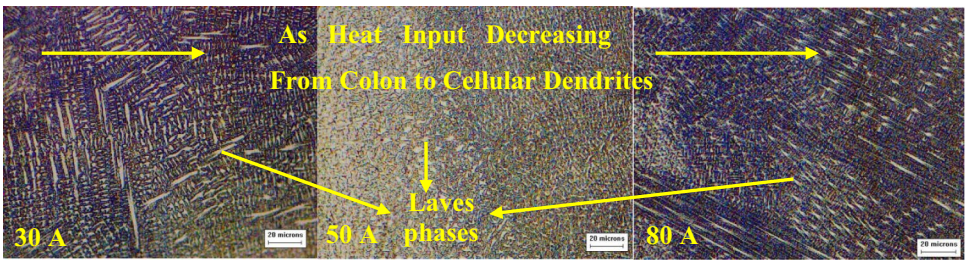


**Fig. 5** FZ on manual welded specimens

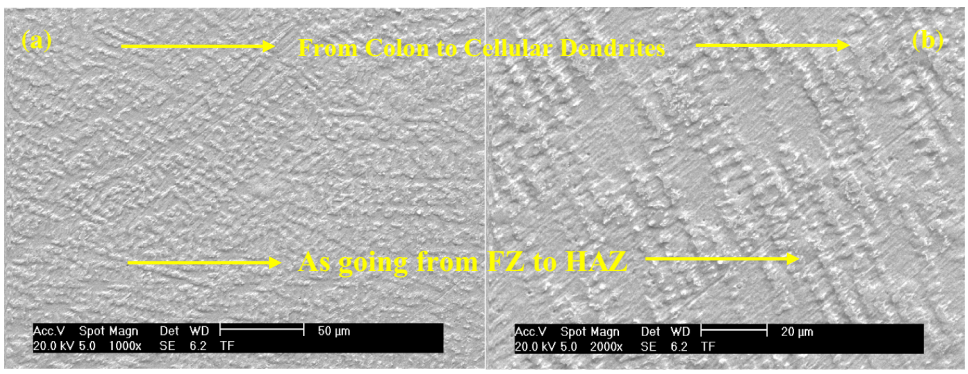


**Fig. 6** **a** FZ—cellular and **b** HAZ—colon dendrites of 80 A manually welded specimen

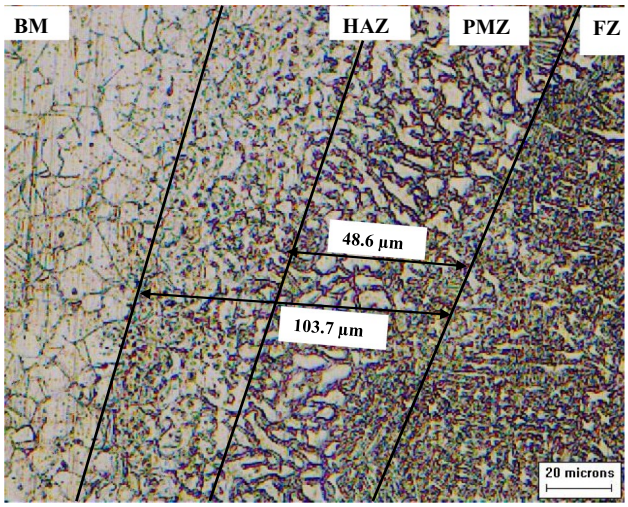


**Fig. 7** Zones on 30 A welded specimen

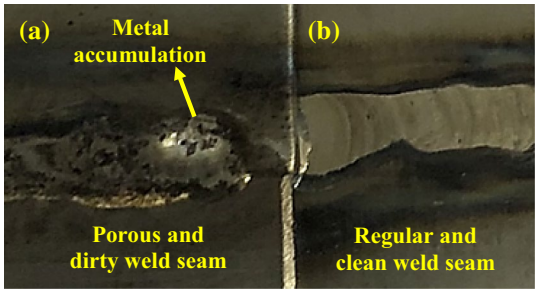


**Fig. 8** **a** Manuel and **b** automatic welding seam macrographs

than colon dendrites do. Hardness increases owing to cellular dendrites also. Unfortunately, it leads to a rigid material that is not generally desired [9, 29, 31]. The widest PMZ was observed on 30 A manually welded specimen which had the highest heat input among all specimens. It had an irregular grain shape and grains were seemed brighter than FZ dendrites. It is commented that the zone was PMZ due to Tanner's prediction [32].

The low welding current extended welding time on 30 A welded specimen, owing to low transverse speed. Low transverse speed led to staying at top temperature longer. As it was stayed at top temperature, the welding seam gets wider, grains grow and PMZ becomes more visible. The wide weld seam and coarse grains decrease strength. PMZ is a very rigid zone, which worsens mechanical properties. The PMZ on 30 A welded specimen was relatively wider than fine noddle-HAZ on 80 A welded specimen (Fig. 4) [32]. HAZ and PMZ were measured as 103.7 µm and 48.6 µm, respectively, in 30 A welded specimen. The widths of these zones are illustrated in Figs. 4 and 7 [5, 30].

### 3.4 Automatic welding effect

Automatization of TIG welding provided several signs of progresses. According to microhardness and tensile strength tests, 80 A was chosen as automatic welding current value. Manually and automatically welded specimens were compared. Less liquid metal accumulation and cleaner weld pool were detected on the automatically welded specimen as shown in Fig. 8. Additionally, automatic welding served a more homogenous weld seam and superb penetration.

Porous and dirty weld seam was observed due to the high temperature conditions facilitating oxidation because it was stayed on the welding pool for a long time. It was difficult to remain welding parameters stable, such as torch angle, transverse speed, and especially arc distance which are listed in Table 3. Although remaining these parameters stable is related to the experience and ability of the welding operator, it is not possible to eliminate all faults and provide excellent weld seam. It can be provided with the only automatization. Welding operator can lead to disappear shielding gas protect over welding pool in fact that was the main reason for porous and dirty weld seam [15, 29, 30]. Bright and green coloured zones were observed between dendrites on the manually welded specimen. Same zones were detected on automatically welded specimen also. But they were observed as finer grains and on fewer ratios. These zones were predicted as the Laves phases (X) as shown in Fig. 9a and b [6, 28, 33]. The dendrites of manually welded specimen were seemed coarser and colon (Y), while the dendrites of automatically welded specimen were finer and cellular (Z).

The automatic welding led to finish welding in a shorter welding time as shown in Table 3. It decreased the heat input, so dendrites could not find time to grow. Cellular dendrites serve higher strength than colon dendrites do. Additionally, the Laves phase occurring due to niobium segregation on Inconel 718 decreases strength. As the heat input increased, the Laves phase had the opportunity to grow in microstructure also. The laves phase grains grew and the Laves phase ratio increased that can be observed in Fig. 9a [13, 33–35].

### 3.5 Microhardness test results

Manually and automatically 80 A welded specimens drew different microhardness profiles than 30 A and 50 A manually welded specimens. Microhardness was measured from BM to FZ as shown in Fig. 10. Microhardness profiles of 80 A welded specimens showed increasing patterns except for weld seam. 80 A welded specimens had microhardness patterns that were expected following the literature [12, 28, 30]. However, it was detected that microhardness increased with welding current. 30 A and 50 A welded specimens served harder HAZ than FZ. These specimens required higher heat

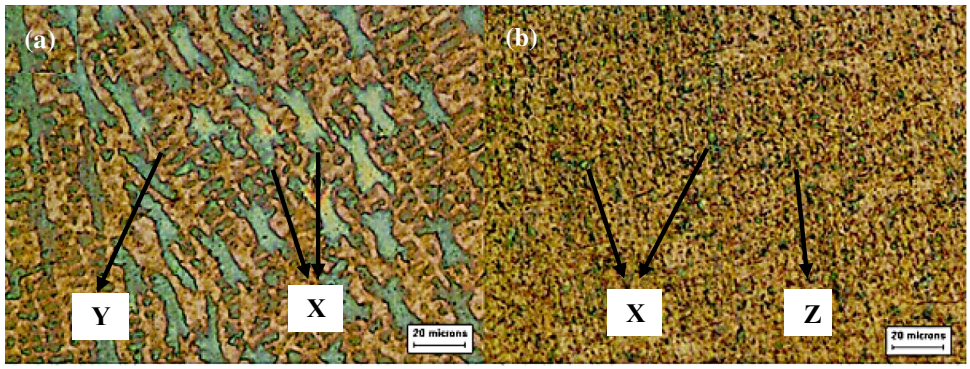


**Fig. 9** **a** 80 A manually and **b** automatically welded FZ microstructures

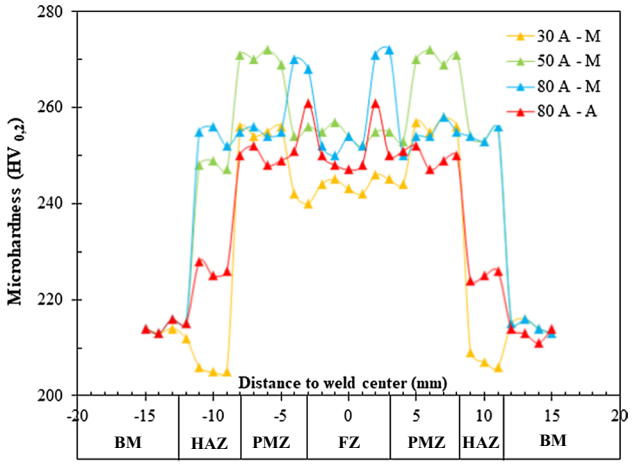


**Fig. 10** Microhardness profiles of the welds

inputs, included wider PMZs, and had increased Laves phase ratios. Alexopoulos et al. had nearly the same microhardness profile in their article which is about fatigue behaviour of TIG welded Inconel 718**.** They claimed that PMZ was slightly harder than the rest. But, they admitted that it was difficult to expose the width of HAZ [36]**.** The microhardness differences between the zones were exposed. They can be observed in Fig. 10. Almost the same microhardness profile was detected in Van et al. study which researched Additive Manufacture (AM) products of Inconel 718. AM serves different cooling rates owing to parameters, such as interpass time and distance from the substrate. Cooling rate resulted in similar microhardness profiles on AM as same as TIG welding regarded with interpass time. They measured microhardness higher because of strengthening heat treatments, that was not applied in present work [37].

The Vickers microhardness profiles served a remarkable result that high heat input led to variable profiles. 30 A and 50 A welded specimens had huge microhardness differences, especially between HAZ and FZ. This fact caused by different cooling rates; in fact, it had more influence than the heat input. 80 A welded specimens showed more homogenous profiles although the microhardness values were higher than the others. Additionally, HAZ was narrower and PMZ had a tendency of disappearing. The 30 A welded specimen which had the highest heat input showed a more ductile HAZ than BM. That showed that annealing existed on HAZ regarded with the long welding time. Although it cooled faster, 80 A automatically welded specimen had lower microhardness scores than the manual one. This fact was associated with the advantages of automatic welding due to it provided homogenous and clean weld seam. The responsible of strength decrease are known as segregation and inclusions, they were minimized by automatization [15, 38, 39].

### 3.6 Ultimate tensile test results

The tensile strength increased as the welding current was elevated. 50 A specimen had deficient strength when was compared with 30 A unexpectedly. Elongation was very low on all manually welded specimens. With automatic welding, the tensile strength and elongation were increased as shown in Table 5. A proceeding paper from Agilan et al. could not detect a remarkable change related to heat input [6]. Progresses on tensile strength and percent elongation are shown in Table 5 owing to adjustments of welding parameters.

30 A manually welded specimen was exposed to excess heat that led to distortions and occurrence of some undesirable phases but it could be an annealing effect for a 1 mm thick specimen. That was the main reason for better tensile test results when 30 and 50 A welded specimens were compared in our opinion. 80 A automatically welded specimen served a superb strength and elongation. It was predicted in Fig. 9 a-b according to microstructure change. Cellular dendrites increased strength and reduced Laves phase ratio led to % 24.40 elongation amounts that was remarkable. It was consistent when compared with the article of Cortes et al. They obtain the elongation as % $25.7 \pm 3.7$ for semi-automatically as-welded specimen [40].

Ramkumar et al. combined Inconel 718 and AISI 416 with laser welding for an article in which they reached similar tensile strength values. Tensile failures were observed in

**Table 5** The ultimate tensile test results

| Specimen | Tensile strength σ-(MPa) | Young module E-(Mpa) | Elongation Δl-(mm) | % Elongation | Max. force F-(N) |
|---|---|---|---|---|---|
| 30 A-M | 430 | 11,670 | 1.23 | 3.97 | 2580 |
| 50 A-M | 403 | 15,564 | 0.91 | 2.94 | 2415 |
| 80 A-M | 454 | 10,333 | 1.40 | 4.52 | 2725 |
| 80 A-A | 686 | 2993 | 7.55 | 24.40 | 4115 |

AISI 416 base metal related to the lower hardness when it was compared with Inconel 718. They also noted that the tensile cracking occurred according to heat input and transverse speed, which was responsible for the Laves phases and microfissuring. As the AISI 416 side of specimens ruptured, the tensile properties of Inconel 718 were obscure [41]. Elongation on all weld seams and failures are illustrated in Fig. 11.

The specimens failed in different zones. 30 and 50 A welded specimens failed near HAZ, while 80 A welded specimens failed in weld centre. These parts of the weld seam had a hardness decrease that can be seen in Fig. 10. Ram et al. detected that the specimens which are solution treated and aged at 980 °C exhibited the best tensile properties and failed in weld centre same as in our present work [42]. Additionally, weld seam widths were measured after rupture. The widths were obtained as 2.97 mm, 2.86 mm, 3.45 mm, and 6.03 mm, respectively. 30 A weld seam was wider than 50 A weld seam that proving the tensile test results (Fig. 9a and b). The elongation on the weld seam increased by nearly %75 owing to automatic welding (Fig. 11c and d). 80 A welded specimens failed in weld centre had also more weld seam elongations. Huda et al. welded X100 pipes with two-pass submerged arc seam method. Failures were detected in HAZ, averagely 1 mm out of the FZ, even in two-pass welded specimens. It is known that the increasing elongation rate indicates more ductile material [43, 44].

### 3.7 Tensile fracture analysis

Fractured surfaces can be observed in Fig. 12 that includes fractured surface of non-welded state along with four welded specimens. The dendrite types varied by heat input were examined previously. The grains for all conditions were consistent with the microstructure observations. Fractured surface of non-welded Inconel 718 showed a conventional high strength and ductile superalloy fracture micrograph. A.Safarzade et. al. detected the same fractured surface on Inconel 625 which is another nickel-based superalloy [45]. Coaxial square grains, wide dimples and fibrous surface can be observed that presents an intergranular ductile fracturing character (Fig. 12a). Fractured surfaces of 30 A and 50 A manually welded specimens were similar to each other. They exhibited colon dendrites with dimples and fracture was intergranular as same as non-welded state (Fig. 12b and c). 80 A manually welded specimen varied with the other manually welded specimens because, it had mostly cellular dendrites (Fig. 12d). Fractured surface of 80 A automatic welded specimen exhibited two different fracture characteristic which were intergranular and transgranular. Fracture similar to cleavage was observed as seen in Fig. 12e. This type of microstructure indicates a brittle fracturing characteristic. Additionally, fracture micrograph of 80 A automatically welded specimen had

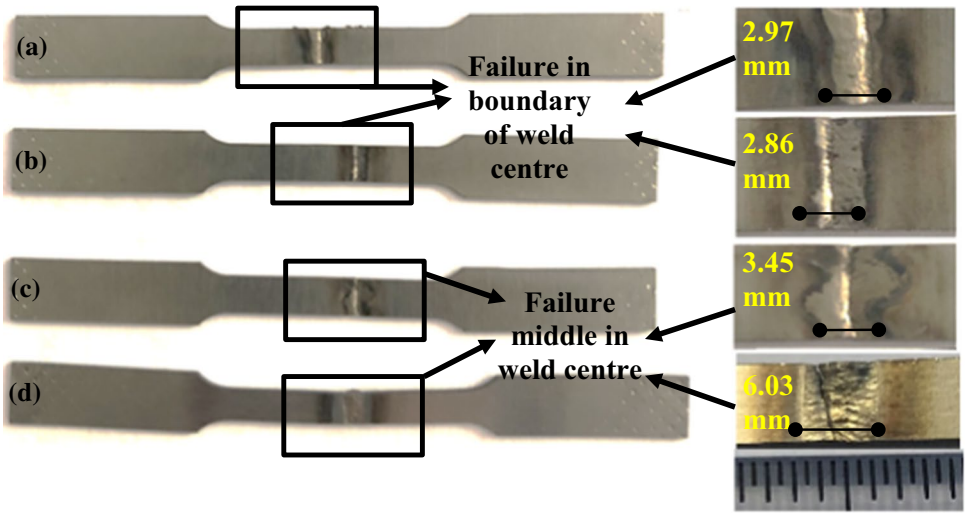


**Fig. 11** **a** 30 A-M, **b** 50 A-M, **c** 80 A-M, **d** 80 A-A failures

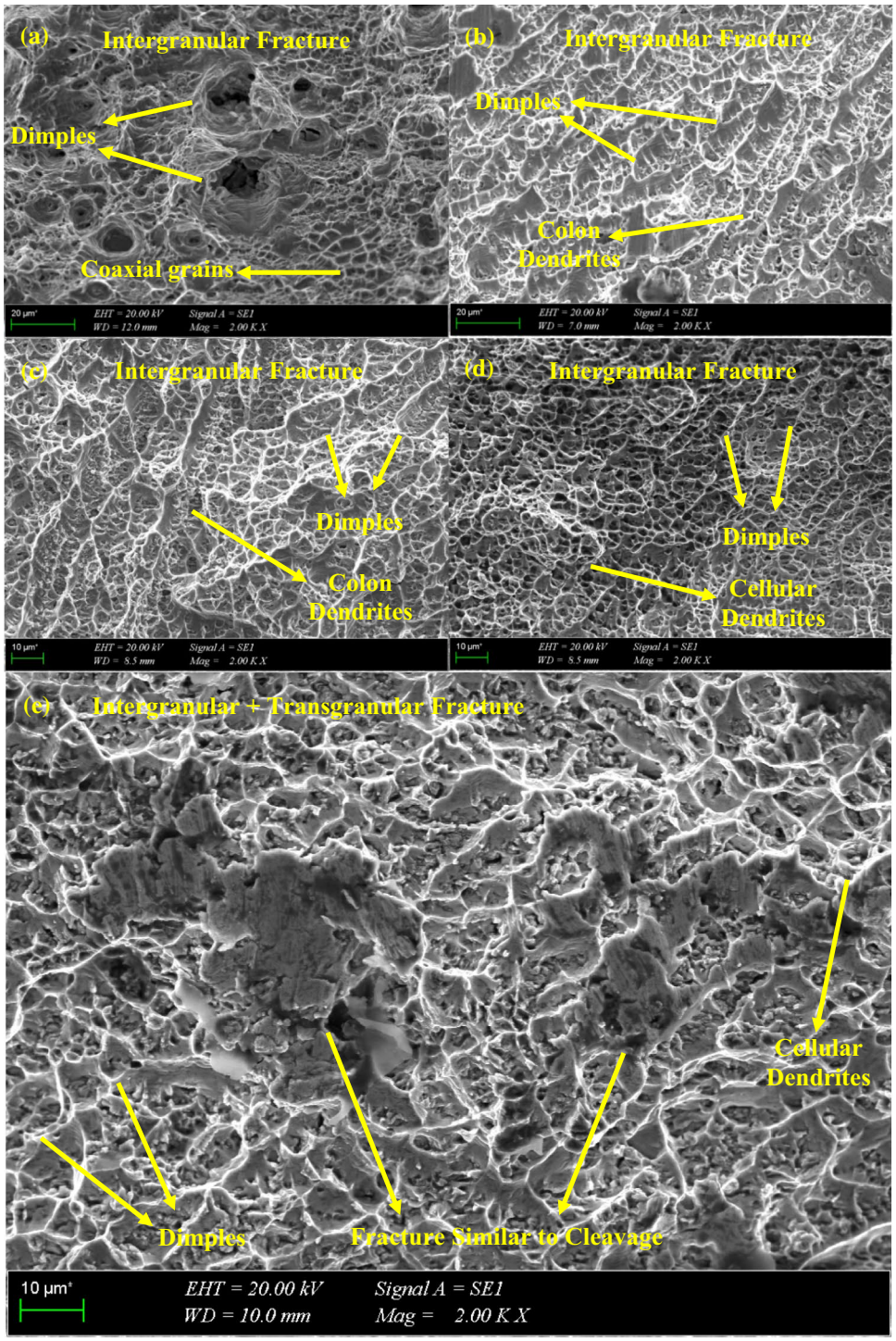


**Fig. 12** Fractured surfaces **a** Non - welded, **b** 30 A manually welded, **c** 50 A manually welded, **d** 80 A manually welded, **e** 80 A automatically welded

dimples that occurred due to ductile fracturing mechanism. Nevertheless, intergranular ductile fracture was the major mechanism. Dendrites were cellular as on 80 A manually welded specimen [45, 46].

The mixed fracture mechanism of brittle and ductile was commended on as a result of automatic welding that served relatively high strength and elongation. Z.K. Teng et al. admitted that the mixture fracturing mechanism exhibited the best fracturing properties [47]. Fractography observations were consistent with the tensile test results and microstructure.

## 4 Conclusions

The data provided by mechanical tests and microstructure observations provided considerable results. Welding current fewer than 30 A resulted in metal accumulations and distortions due to low transverse speed. Current values upper 80 A resulted in melted zones, because of extreme energy that was provided. However, heat input was decreased by nearly %25. HAZ and PMZ widths decreased nearly to half due to low-heat input conditions. Grains were finer and the Laves phase ratio was fewer. Automatic welding provided reduced microhardness especially on HAZ and it minimized PMZ width for all conditions. High heat input caused annealing on 30 A welded specimen. 30 A welded specimen was subject of elongation more than 50 A welded specimen. It proves the annealing effect. 80 A manually welded specimen had better strength and elongation. 80 A automatically welded specimen exhibited excellent tensile and elongation properties as a result of elimination welding operator mistakes. Owing to the automatic welding, the tensile strength was increased approximately %50, while the elongation increased to five times. The high heat input caused failures near HAZ at 30 A and 50 A welded specimens. 80 A welded specimens ruptured in FZ owing to heat input decrease. Manually welded specimens showed ductile fracturing character while automatically welded specimen had a mixed of fracturing mechanism.

## References


1. Damodaram, R.; Ganesh Sundara Raman, S.; Prasad Rao, K.: Effect of post-weld heat treatments on microstructure and mechanical properties of friction welded alloy 718 joints. Mater. Des. **53**, 954–961 (2014). https://doi.org/10.1016/j.matdes.2013.07.091
2. Group F. BLISK. Group, Farin Web Page n.d. https://www.farinia.com/additive-manufacturing/3d-materials/inconel-718-aerospace-additive-manufacturing.
3. Wang, Q; Sun, D.L.; Na, Y.; Zhou, Y.; Wang, X.L.H.J.: Effects of TIG welding parameters on morphology and mechanical properties of welded joint of Ni-base superalloy. Procedia. Eng. **10**, 37–41 (2011). https://doi.org/10.1016/j.proeng.2011.04.009
4. Gordine, J.: Welding of ınconel 718. Weld. Res. Suppl. Weld. J. **49**, 531–537 (1970)
5. Gordine, J.: Some problems in welding ınconel 718. Weld Res Suppl **50**, 480-s (1971)
6. Agilan, M.; Venkateswaran, T.; Sivakumar, D.; Pant, B.: Effect of heat input on microstructure and mechanical properties of inconel-718 EB welds. Proc. Mater Sci **5**, 656–662 (2014). https://doi.org/10.1016/j.mspro.2014.07.312
7. Schirra JJ; Caless RH; Hatala RW. The Effect of Laves Phase on the Mechanical Properties 1991:375–88.
8. Janaki Ram, G.D.; Venugopal Reddy, A.; Prasad Rao, K.; Madhusudhan, R.G.: Microstructure and mechanical properties of Inconel 718 electron beam welds. Mater Sci Technol **21**, 1132–1138 (2005). https://doi.org/10.1179/174328405X62260
9. Lm B; Inconel; Mekan. Elektron Işını ve TIG Kaynağı Yöntemleriyle Birleştirilmiş Inconel Malzemenin Özelliklerinin Karşılaştırılması 2009;2:1–6
10. Hong, T.S.; Ghobakhloo, M.; Khaksar, W.: Robotic welding technology. Comprehen. Mater. Process. (2014). https://doi.org/10.1016/B978-0-08-096532-1.00604-X
11. Erden, M.S.; Marić, B.: Assisting manual welding with robot. Robot. Comput. Integr. Manuf. **27**, 818–828 (2011). https://doi.org/10.1016/j.rcim.2011.01.003
12. Kumar, H.; Ahmad, G.N.; Singh, N.K.: Activated flux TIG welding of Inconel 718 super alloy in presence of tri-component flux. Mater. Manuf. Process **34**, 216–223 (2019). https://doi.org/10.1080/10426914.2018.1532581
13. Ram, G.D.J.; Reddy, A.V.; Rao, K.P.; Reddy, G.M.: Control of laves phase in inconel 718 GTA welds with current pulsing. Sci. Technol. Weld. Join. **9**, 390–398 (2004). https://doi.org/10.1179/136217104225021788
14. Kurt A. KAYNAK METALURJİSİ 2013:1–151.
15. Kumar, T.; Balasubramanian, V.; Senthilkumar, T.: Influences of pulsed current tungsten inert gas welding parameters on the tensile properties of AA 6061 aluminium alloy. Mater. Des. **28**, 2080–2092 (2007). https://doi.org/10.1016/j.matdes.2006.05.027
16. Standard E. TS EN ISO 5817:2014 2014
17. TSE. TS EN ISO 6848 2010. https://intweb.tse.org.tr/Standard/Standard/Standard.aspx?081118051115108051104119110104055047105102120088111043113104073087106069070073069097101085122054.
18. Standard TO, Standard N. Standard Test Methods for Tension Testing of Metallic Materials 1. Astm 2009;i:1–27.
19. Standard A. ASTM E-407 - 07(2015) e1 2015. https://www.astm.org/Standards/E407.
20. Composition C. Nickel Alloy 718 Data Sheet 2018;718. 1.888.282.3292.
21. Nevcanoğlu A; Salman S; Pazarlıoğlu S. TIG KAYNAĞI YÖNTEMİ İLE BİRLEŞTİRİLMİŞ INCONEL 718 SÜPER ALAŞIM MALZEMENİN KAYNAK SONRASI ÖZELLİKLERİNİN İNCELENMESİ 2019.
22. Anuradha, M.; Das, V.C.; Susila, P.; Cheepu, M.; Venkateswarlu, D.: Effect of welding parameters on TIG welding of inconel 718 to AISI 4140 steel. Trans. Indian Inst. Met. **73**, 1515–1520 (2020). https://doi.org/10.1007/s12666-020-01926-8
23. Sambherao, P.A.B.: Use of activated flux for increasing penetration in austenitic stainless steel while performing GTAW. Int. J. Emerg. Technol. Adv. Eng. **3**, 520–524 (2013)
24. Agilan, M.; Venkateswaran, T.; Sivakumar, D.; Pant, B.: Effect of post weld heat treatment on mechanical properties and microstructure of nickel based super alloy welds. Adv. Mater. Res. **585**, 435–439 (2012). https://doi.org/10.4028/www.scientific.net/amr.585.435
25. Jose, P.J; Dev, M.: Comprehensive analysis of TIG welded inconel-718 alloy for different heat input conditions. Int. J. Eng. Technol. **7**(3.6), 206–209 (2018). https://doi.org/10.14419/ijet.v7i3.6.14971
26. Venukumar, S.; Sarkar, P.; Sashank, J.S.; Sampath, P.; Saikiran, K.: Microstructural and mechanical properties of Inconel 718 TIG weldments. Mater. Today Proc. **5**, 8480–8485 (2018). https://doi.org/10.1016/j.matpr.2017.11.544
27. Zhang, D.; Niu, W.; Cao, X.; Liu, Z.: Effect of standard heat treatment on the microstructure and mechanical properties of selective laser melting manufactured Inconel 718 superalloy. Mater. Sci. Eng. A (2015). https://doi.org/10.1016/j.msea.2015.06.021
28. Zwilsky KM; President, Internatıonal A, Langer El; Director M, Internatıonal A. ASM Metals Handbook, Vol 01. Technology 2001;1:3470. https://doi.org/10.1016/S0026-0576(03)90166-8.
29. Tao, P.; Li, H.; Huang, B.; Hu, Q.; Gong, S.; Xu, Q.: The crystal growth, intercellular spacing and microsegregation of selective

laser melted Inconel 718 superalloy. Vacuum **159**, 382–390 (2019). https://doi.org/10.1016/j.vacuum.2018.10.074
30. Ye, X.; Hua, X.; Wang, M.; Lou, S.: Controlling hot cracking in Ni-based Inconel-718 superalloy cast sheets during tungsten inert gas welding. J. Mater. Process Technol. **222**, 381–390 (2015). https://doi.org/10.1016/j.jmatprotec.2015.03.031
31. Ramkumar, K.D.; Kumar, B.M.; Krishnan, M.G.; Dev, S.; Bhalodi, A.J.; Arivazhagan, N.; et al.: Studies on the weldability, microstructure and mechanical properties of activated flux TIG weldments of Inconel 718. Mater. Sci. Eng. A **639**, 234–244 (2015). https://doi.org/10.1016/j.msea.2015.05.004
32. Tanner, DWJ.: Life assessment of welded INCONEL 718 at high temperature. PhD thesis, University of Nottingham (2009). Access from the University of Nottingham repository: http://eprints.nottingham.ac.uk/10796/1/DWJ_Tanner_PhD_Thesis.pdf
33. Karthick, B.; ArunKannan; Manojkumar, S.: Pulsed TIG welding—a review. Int. Res. J. Advan. Sci. Hub. (IRJASH) **1**, 42–49 (2019) e-ISSN: 2582-4376
34. Qi, H.; Azer, M.; Ritter, A.: Studies of standard heat treatment effects on microstructure and mechanical properties of laser net shape manufactured INCONEL 718. Metall. Mater. Trans. A Phys. Metall. Mater. Sci. **40**, 2410–2422 (2009). https://doi.org/10.1007/s11661-009-9949-3
35. GELİŞ ÖGK. Kaynak Teknolojisi. vol. 8. Ağrı İbrahim Çeçen Üniversitesi Meslek Yüksek Okulu; 2014.
36. Alexopoulos, N.D.; Argyriou, N.; Stergiou, V.; Kourkoulis, S.K.: Fatigue behavior of Inconel 718 TIG welds. J. Mater. Eng. Perform. **23**, 2973–2983 (2014). https://doi.org/10.1007/s11665-014-1028-2
37. Van, D.; Dinda, G.P.; Park, J.; Mazumder, J.; Lee, S.H.: Enhancing hardness of Inconel 718 deposits using the aging effects of cold metal transfer-based additive manufacturing. Mater. Sci. Eng. A **776**, 139005 (2020). https://doi.org/10.1016/j.msea.2020.139005
38. Volume, T.H.E.; Were, C.; Leroy, D.; Siewert, T.A.; Liu, S.; Edwards, G.R.: ASM Handbook, Welding, Brazing, and Soldering, Vol. 6, p. 2873. ASM International (1993) https://doi.org/10.2134/jeq2003.8650
39. Chlebus, E.; Gruber, K.; Kuźnicka, B.; Kurzac, J.; Kurzynowski, T.: Effect of heat treatment on the microstructure and mechanical properties of Inconel 718 processed by selective laser melting. Mater. Sci. Eng. A **639**, 647–655 (2015). https://doi.org/10.1016/j.msea.2015.05.035
40. Cortés, R.; Barragán, E.R.; López, V.H.; Ambriz, R.R.; Jaramillo, D.: Mechanical properties of Inconel 718 welds performed by gas tungsten arc welding. Int. J. Adv. Manuf. Technol. **94**, 3949–3961 (2018). https://doi.org/10.1007/s00170-017-1128-x
41. Sidharth, D.; Phani Prabhakar, K.V.; Rajendran, R.; Narayanan, S.: Microstructure and properties of inconel 718 and AISI 416 laser welded joints. J. Mater. Process Technol. **266**, 52–62 (2019). https://doi.org/10.1016/j.jmatprotec.2018.10.039
42. Janaki Ram, G.D.; Venugopal Reddy, A.; Prasad Rao, K.; Reddy, G.M.; Sarin Sundar, J.K.: Microstructure and tensile properties of Inconel 718 pulsed Nd-YAG laser welds. J. Mater. Process Technol. **167**, 73–82 (2005). https://doi.org/10.1016/j.jmatprotec.2004.09.081
43. Huda, N.; Gianetto, J.; Ding, Y.; Lazor, R.; Gerlich, A.P.: Investigation of local tensile strength and ductility properties of an X100 submerged arc seam weld. Mater. Sci. Eng. A **768**, 138475 (2019). https://doi.org/10.1016/j.msea.2019.138475
44. Mamat, M.F.; Hamzah, E.; Ibrahim, Z.; Rohah, A.M.; Bahador, A.: Effect of filler metals on the microstructures and mechanical properties of dissimilar low carbon steel and 316L stainless steel welded joints. Mater. Sci. Forum **819**, 57–62 (2015). https://doi.org/10.4028/www.scientific.net/MSF.819.57
45. Safarzade, A.; Sharıfıtabar, M.; Shafıee, A.M.: Effects of heat treatment on microstructure and mechanical properties of Inconel 625 alloy fabricated by wire arc additive manufacturing process. Trans. Nonferrous Met. Soc. China English Ed **30**, 3016–3030 (2020). https://doi.org/10.1016/S1003-6326(20)65439-5
46. Li, G.; Huang, J.; Wu, Y.: An investigation on microstructure and properties of dissimilar welded Inconel 625 and SUS 304 using high-power CO2 laser. Int J Adv Manuf Technol **76**, 1203–1214 (2015). https://doi.org/10.1007/s00170-014-6349-7
47. Teng, Z.K.; Liu, C.T.; Ghosh, G.; Liaw, P.K.; Fine, M.E.: Effects of Al on the microstructure and ductility of NiAl-strengthened ferritic steels at room temperature. Intermetallics **18**, 1437–1443 (2010). https://doi.org/10.1016/j.intermet.2010.03.026